NANO LETTERS

Letter

pubs.acs.org/NanoLett

Rapid Identification of Stacking Orientation in Isotopically Labeled Chemical-Vapor Grown Bilayer Graphene by Raman Spectroscopy

Wenjing Fang,[†] Allen L. Hsu,[†] Roman Caudillo,[§] Yi Song,[†] A. Glen Birdwell,[∥] Eugene Zakar,[∥] Martin Kalbac,[⊥] Madan Dubey,[∥] Tomás Palacios,[†] Millie S. Dresselhaus,[†,‡] Paulo T. Araujo,*[,†] and Jing Kong*[,†]

[†]Department of Electrical Engineering and Computer Sciences and [‡]Department of Physics, Massachusetts Institute of Technology, Cambridge, Massachusetts 02139, United States

[§]Intel Corporation, Components Research, 2501 NW 229th Avenue, RA3-252, Hillsboro, Oregon 97124, United States

[∥]U.S. Army Research Laboratory, 2800 Powder Mill Road, Adelphi, Maryland 20783, United States

[⊥]J. Heyrovský Institute of Physical Chemistry, Academy of Sciences of the Czech Republic, v.v.i., Dolejskova 3, CZ-18223 Prague 8, Czech Republic

Supporting Information

ABSTRACT: The growth of large-area bilayer graphene has been of technological importance for graphene electronics. The successful application of graphene bilayers critically relies on the precise control of the stacking orientation, which determines both electronic and vibrational properties of the bilayer system. Toward this goal, an effective characterization method is critically needed to allow researchers to easily distinguish the bilayer stacking orientation (i.e., AB stacked or turbostratic). In this work, we developed such a method to provide facile identification of the stacking orientation by isotope labeling. Raman spectroscopy of these isotopically labeled bilayer samples shows a clear signature associated with AB stacking between layers, enabling rapid differentiation between turbostratic and AB-stacked bilayer regions. Using this method, we were able to characterize the stacking orientation in bilayer graphene grown through Low Pressure Chemical Vapor Deposition (LPCVD) with enclosed Cu foils, achieving almost 70% AB-stacked bilayer graphene. Furthermore, by combining surface sensitive fluorination with such hybrid $^{12}C/^{13}C$ bilayer samples, we are able to identify that the second layer grows underneath the first-grown layer, which is similar to a recently reported observation.

KEYWORDS: *AB-stacked bilayer graphene, carbon isotope, Raman spectroscopy, growth mechanism, fluorination*

Bilayer graphene is an important material not only for fundamental physics but also for potential carbon-enabled device applications.[1−4] The relative stacking orientation between the individual graphene sheets plays a significant role on the electronic properties of the resulting bilayer graphene. For instance, AB-stacked bilayers obtained from highly oriented pyrolytic graphite (HOPG) can exhibit a tunable band gap of up to 250 meV with an applied external electric field, which can be used for infrared light detection[4] high on/off ratio digital graphene-based transistors,[5] as well as serve as a model system to study tunable Fano resonances.[6] On the other hand, large-area turbostratic bilayers do not exhibit a tunable band gap but instead can reduce a film's overall sheet resistance, which can be useful for transparent conductive electrode applications such as touch screens and solar cells.[7,8] Consequently, many groups have explored a variety of methods for producing large-area bilayer graphene. Various transition metal catalysts such as Ru(0001),[9] Ir(111),[10] Cu−Ni alloys,[11] Cu[12,13] have been able to achieve Bernal stacked bilayer graphene, while methods utilizing only Ni have generated turbostratically stacked bilayer graphene.[14,15] The growth mechanisms among these various substrates range from surface limited growth to carbon precipitation, and one important growth question still remains elusive: how can the stacking orientation (turbostratic versus AB stacking) be controlled? To address this question, a fast and effective method of analyzing stacking orientation in bilayer graphene is highly desirable. Traditionally a combination of Raman spectroscopy and transmission electron microscopy (TEM) have been used to identify the stacking orientation.[16] These methods generally rely on evaluating the full width at half-maximum (fwhm) of the G′ Raman peak combined with selected area electron diffraction (SAED) patterns to verify the stacking orientation.[17] However, SAED is a time-consuming process and only examines a relatively small sample region (100 nm ∼ 1 μm) and the Raman spectra do not always provide a clear signature for identifying the type of bilayer stacking. Finding an efficient and confident method to assess the area percentage of AB-stacked bilayer versus turbostratic bilayer in a graphene sample will be critical for the controlled synthesis in the future.

In this work, we have developed such a method by combining isotope labeling and Raman spectroscopy. Large-area AB-stacked bilayer graphene is grown using a Cu enclosure method.[18] The use of isotopic labeling for CVD graphene synthesis was first introduced to distinguish the difference

Received: December 20, 2012
Revised: March 3, 2013
Published: March 7, 2013

dx.doi.org/10.1021/nl304706j | *Nano Lett.* 2013, 13, 1541−1548

between the growth mechanism of graphene on Cu and Ni[18] and was later used for doping studies of graphene.[19] More recently it was also used to identify the stacking sequence of bilayer graphene grown in the inside of the Cu enclosure.[20] The bilayer graphene studied in our work is from the outside of the Cu enclosure, nevertheless, we have obtained the same conclusion regarding the stacking sequence, that is, the second layer of graphene grows underneath the first layer. By sequentially flowing $^{12}CH_4$ and $^{13}CH_4$, we were able to produce bilayer graphene domains where the first grown graphene layer consists solely of ^{12}C and the second layer consists of both ^{12}C and ^{13}C. Upon analysis of the G′ peak, we found a clear feature in the Raman spectra that, supported by TEM electron-diffraction studies, enables us to easily differentiate between AB-stacked and turbostratic bilayer graphene. Utilizing this feature we were able to perform rapid large-area identification of the stacking orientation type (AB- or turbostratic) of bilayer graphene. Furthermore, the presence of interlayer vibrational Raman peaks was also observed, which is a spectroscopic signature of the AB-stacking orientation in AB-stacked bilayer graphene.

Bilayer Graphene Synthesis. Here we utilized the Cu enclosure method for the growth of large-domain size (>20 μm) bilayer graphene by LPCVD. This method is based on the Cu envelope/enclosure method developed by Li et al. (see the Methods for details).[21] However, we focused on the graphene grown on the outside surface rather than the inside surface of the Cu enclosure.[22] To study the growth effect of the Cu enclosure on bilayer graphene, graphene films on flat and enclosed substrates were grown side by side at 1000 °C using 1.5 sccm CH_4 and 35 sccm H_2 for different lengths of time. In Figure 1, the SEM images show that in the early growth stages (within the first 5 min), the monolayer graphene coverage was not complete. In the center of the individual graphene domains, we observed darker regions, which correspond to bilayer or multilayer graphene. We found that these bilayers or multilayers nucleate at the same time as the monolayer graphene. In addition, at this early stage (~5 min) the nucleation density and the size of the bilayer graphene domains were similar on both flat and enclosed substrates. As the growth progresses further, individual monolayer graphene domains coalesced into a single monolayer. It should be noted that once the monolayer coverage was complete, we observed a "self-limiting" effect for the growth rate of the bilayer graphene on the flat substrate, consistent with previous reports.[23] On the other hand, under this same condition bilayer graphene on the outside of the Cu enclosure continued to grow until it finally saturated at about 70% total coverage on the outside surface of the Cu enclosure.

Raman and TEM analysis. Using the same enclosure method, we sequentially controlled the introduction of ^{12}C and ^{13}C in order to grow $^{12}C/^{13}C$ hybrid bilayer graphene. We introduced $^{12}CH_4$ for 90 s to grow the continuous monolayer and then purged the system for 5 min with 100 sccm Ar/10 sccm H_2 to reduce intermixing between the isotopes. After purging, we introduced $^{13}CH_4$ for 30 min to increase the domain size of the bilayer. Figure 2b shows the optical images of the transferred bilayer graphene grown on the outside of the Cu enclosure using 1.5 sccm CH_4/ 50 H_2 at 1035 °C. Figure 2c presents a two-dimensional Raman map showing the integrated G peak intensity of ^{12}C (1580–1620 cm^{-1}) and ^{13}C (1510–1550 cm^{-1}), respectively. In the G peak mapping for ^{12}C, we observed that the monolayer graphene is continuous and composed entirely of ^{12}C. The higher G peak intensity regions

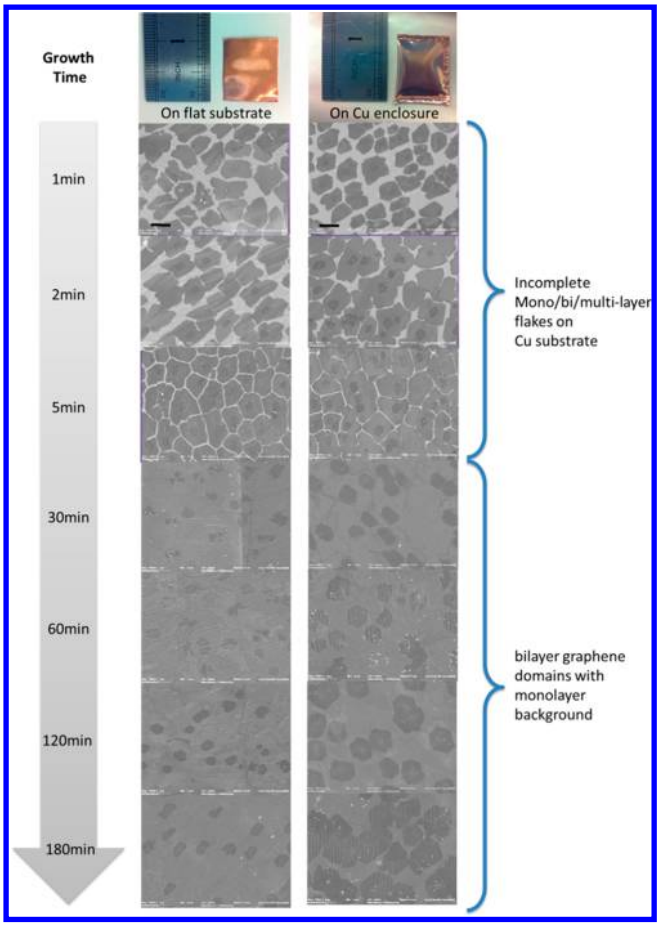

Figure 1. Comparison of graphene film growth as a function of time. Samples were imaged on both flat Cu substrates and the outside surface of Cu enclosures at 1000 °C using 1.5 sccm CH_4 and 35 sccm H_2. The SEM images all have the same magnification (10K×) and the scale bars are 10 μm.

in the center corresponds to the $^{12}C/^{12}C$ bilayer, which nucleated with the monolayer domain at the same time as shown previously in Figure 1. In the G peak mapping for ^{13}C, the bright regions show the distribution of ^{13}C while the black regions indicate the absence of ^{13}C. After the first 90 s of growth using $^{12}CH_4$ and purging, the $^{13}CH_4$ decomposed and attached to the edges of already existing hexagonal bilayer graphene domains. Figure 2a presents the typical Raman spectra taken from different locations in Figure 2b. To differentiate between various stacking orientations and layers, we adopt a naming convention consisting of "Isotope Stacking orientation-Number of layers"; for example, $^{12}C/^{12}C$ AB-BLG denotes AB-stacked bilayer graphene composed of ^{12}C only. In Figure 2a, the black spectra show the reference monolayer spectra of ^{12}C and ^{13}C. The Raman spectrum of the ^{13}C monolayer graphene (^{13}C SLG) exhibited a downshift of all the Raman features compared to the ^{12}C monolayer graphene (^{12}C SLG), due to the different phonon energies resulting from the different ^{12}C and ^{13}C masses.[18] The blue spectra in Figure 2a were taken from the center of the two bilayer domains, which are composed of ^{12}C only. The dotted blue-line spectrum in Figure 2a exhibits a G′ peak with a fwhm of ~28 cm^{-1} and a G′/G peak intensity ratio of ~6.2, suggesting it is a turbostratic bilayer system. On the other hand, the solid blue-line spectrum exhibited a G′ peak with a fwhm of ~64 cm^{-1} and a lower G′/G intensity ratio of ~1.56. This strongly suggested the

dx.doi.org/10.1021/nl304706j | Nano Lett. 2013, 13, 1541–1548

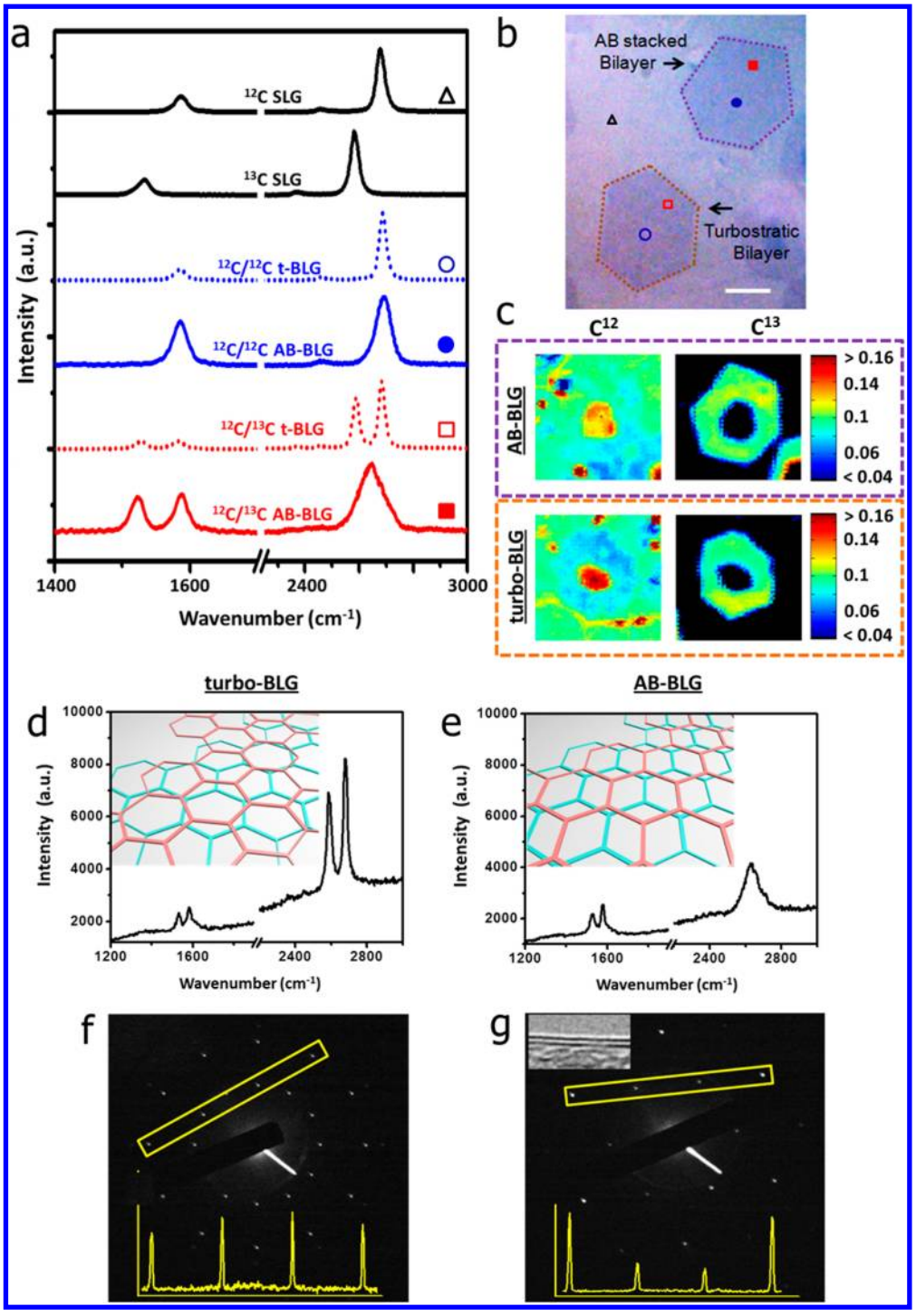

Figure 2. Raman spectroscopy and TEM characterization of bilayer graphene. (a) Raman spectra of a ^{12}C monolayer and ^{13}C monolayer (black), ^{12}C/^{12}C turbostratic bilayer (dotted blue), ^{12}C/^{12}C AB-stacked bilayer (solid blue), ^{12}C/^{13}C turbostratic bilayer (dotted red) and ^{12}C/^{13}C AB-stacked bilayer (solid red) taken from (b). (b) Optical image of bilayer graphene transferred on Si/SiO_2. Scale bar is 5 μm. The bilayer domain outlined by the purple dots is AB-stacked and another domain by orange is turbostratic. (c) Integrated G peak intensity of ^{12}C (1580−1620 cm^{-1}) or ^{13}C (1510−1550 cm^{-1}), respectively, for domains in (b). (d,e) Two representative Raman spectra taken from suspended bilayer graphene on a SiN TEM grid. The insets show the stacking orientation. (f,g) The SAED patterns for (d,e) and the corresponding intensity profiles along the yellow lines. Inset in upper left corner of (g) is a TEM image, which indicates the number of layers.

occurrence of AB stacking, even though some of the common features and asymmetries in the spectrum were not as clear as the ones observed in exfoliated Bernal AB-stacked graphene.[14] Finally, the red spectra in Figure 2a were taken from the outer region of the bilayer domains where each layer was solely composed of ^{12}C or ^{13}C. Both spectra showed a clear separation of the G peaks associated with each C isotope at 1523 cm^{-1} and 1588 cm^{-1}, a combination of one ^{12}C layer and another ^{13}C layer.[24] However, while both red spectra clearly showed two types of graphene, the shape of their G′ peaks differed significantly. The dotted red-line spectrum from the turbostratic bilayer graphene sample shows two distinct G′

dx.doi.org/10.1021/nl304706j | *Nano Lett.* 2013, 13, 1541−1548

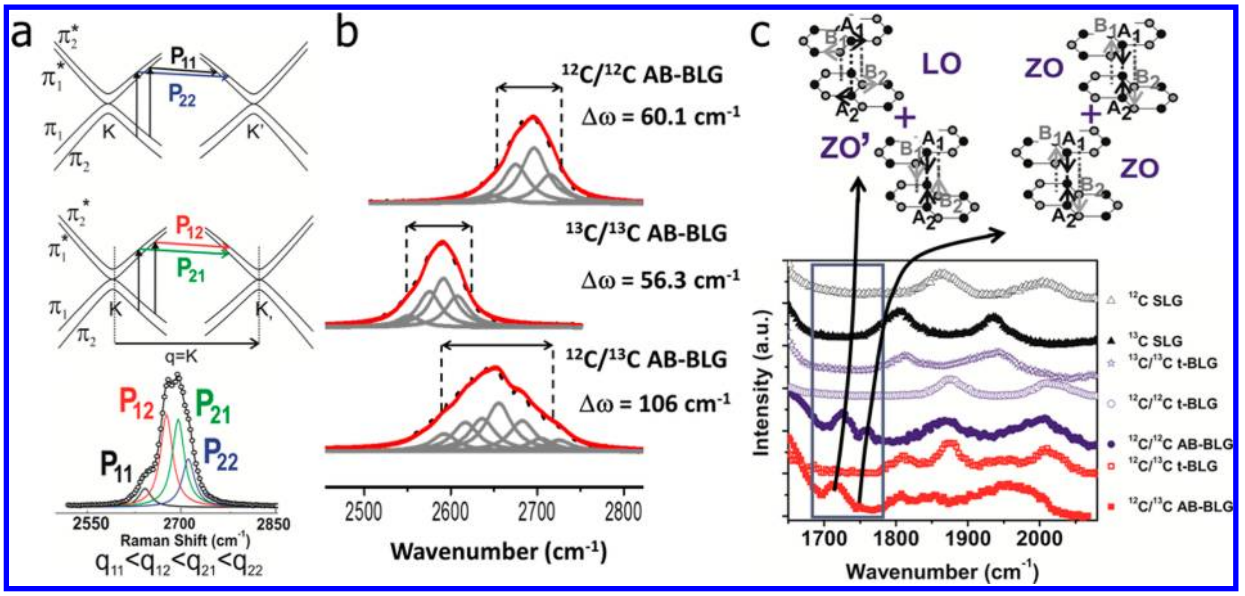

Figure 3. Raman signatures for the AB-stacked BLG structures. (a) Double resonance Raman processes that give rise to the four peaks in the G′ band in AB-BLG obtained from HOPG. The inset shows the G′ band measured with the 532 nm laser line and the four peaks corresponding to each resonance process: P_{11} (black line), P_{12} (red line), P_{21} (green line), and P_{22} (blue line) with the relative magnitudes of the four phonon wavevectors **q** shown. (b) Peak fitting of the G′ band for $^{12}C/^{12}C$ AB-BLG, $^{13}C/^{13}C$ AB-BLG, and $^{12}C/^{13}C$ AB-BLG. As expected, the G′ fwhm for the $^{12}C/^{13}C$ AB-BLG sample is almost twice the G′ fwhm of the $^{12}C/^{12}C$ AB-BLG and $^{13}C/^{13}C$ AB-BLG samples. (c) Raman spectra of the combination modes in SLG and BLG systems from CVD-grown graphene. The spectral region in the frequency range from 1650 to 1750 cm^{-1} (see the region delimited by the gray box) shows the combination of mode LO+ZO′ and 2ZO, which are only observed in the two AB-BLG systems.

bands, which is to be expected for two electronically decoupled layers, while the solid red-line spectrum shows only a singular, but broader G′ band with a fwhm of ∼106 cm^{-1}, almost twice the fwhm observed for the $^{12}C/^{12}C$ AB-BLG. We attribute this broad G′ band to an interlayer interaction, which appears due to a similar stacking as observed by the Raman spectra of $^{12}C/^{12}C$ AB-BLG in the center panel.

TEM and SAED were used to further confirm the stacking orientation of the graphene bilayers. The TEM and SAED sample was prepared by transferring graphene films grown under the same conditions as the Raman samples discussed above onto SiN TEM substrates. Raman mapping was performed on suspended bilayer graphene samples, followed by SAED over the same region for more than 20 locations. An example is shown in Figure 2d for a Raman spectra with two distinct G′ bands; the electron diffraction pattern always generates two sets of monolayer graphene diffraction patterns. By examining the intensity profile of the diffraction spots, we learned that the bilayers were composed of two monolayers of turbostratic graphene. In contrast, for a broad G′ Raman spectra, only a single diffraction pattern was observed. Plotting the line intensity of the diffraction peaks, we found that the ratio of intensity of the equivalent planes $\{1\bar{2}10\}$ over the inner peaks from $\{1\bar{1}00\}$ is about 2, which confirms AB stacking.[25−27]

To explain the origin of the broad G′ band for $^{12}C/^{13}C$ AB-BLG in Figure 2, we must first understand the phonon structure changes in $^{12}C/^{12}C$ AB-BLG. The AB-BLG system can be understood as a weak coupling between the six phonon modes of the bottom layer and the six phonon modes of the top layer (Supporting Information). Around the high-symmetry *K*-point the iTO (in-plane transverse optical mode) mode describes the G′ Raman feature (the G′ peak is a double phonon resonant Raman process involving two iTO phonons around the *K*-point[28−30]). As largely discussed in the literature,[28,31,32] for $^{12}C/^{12}C$ AB-BLG, the G′ feature is shown to be comprised of four peaks due to different resonances of the iTO mode with the different electronic sub-bands, as shown in Figure 3a.[28,31,32] Extending the arguments further to the $^{12}C/^{13}C$ BLG system, in the case of the $^{12}C/^{13}C$ t-BLG system, we still have the six phonon modes of the bottom layer and the six phonon modes of the top layer. However, the phonon modes are no longer degenerate (the degeneracy is broken due to the different masses of the carbon isotopes), but their electronic dispersions are kept linear (Dirac-like dispersion) and independent, and therefore they vibrate with frequencies that are related by

$$\omega(^{13}C) = \sqrt{\frac{12}{13}}\,\omega(^{12}C)$$

where $\omega(^{13}C)$ and $\omega(^{12}C)$ denote the phonon mode frequencies in the ^{13}C and ^{12}C layers, respectively. This fully explains the consistent shifts in the system $^{12}C/^{13}C$ t-BLG observed in Figure 2a. For a $^{12}C/^{13}C$ AB-BLG system, we still will observe two G band features (a first order Raman process around the Γ-point), which are now a symmetric and anti-symmetric combination among the in-plane longitudinal, LO, and tranversal, TO, phonon modes from the top and bottom layers since the different phonons due to the different masses play a larger role than the change in electronic dispersion. However, for the G′ band the situation is slightly different due to the differences in the ^{12}C and ^{13}C masses, the iTO modes from the top and bottom layers are no longer unique at the *K*-point. However, similar to what happens for the $^{12}C/^{12}C$ AB-BLG system, the electronic dispersion is still a hyperbolic dispersion with two different sub-bands (around the *K*-point), since in this isotopic system, opposite to what happens to the vibrational properties, the electronic properties are maintained. Therefore, instead of four resonances with the iTO mode, we could observe up to eight different resonances, in which each

dx.doi.org/10.1021/nl304706j | *Nano Lett.* 2013, 13, 1541−1548

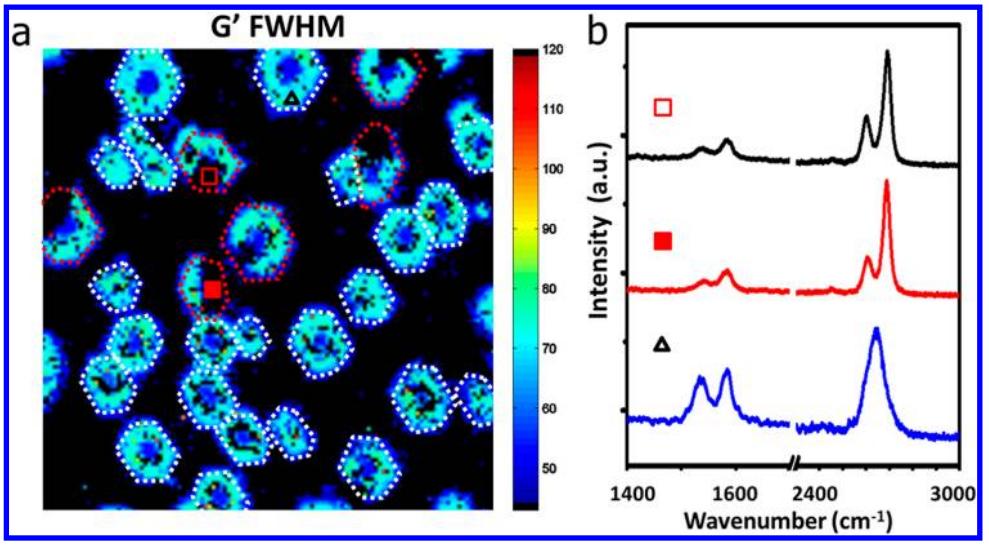

Figure 4. Raman spectroscopy of bilayer graphene. (a) Raman mapping of integrated G′ fwhm of $^{12}C/^{13}C$ BLG over an area of 60 μm by 60 μm. $^{12}C/^{13}C$ AB-BLG (dotted white-line) and regions containing some $^{12}C/^{13}C$ t-BLG (dotted red-line) are highlighted. (b) Representative Raman spectra taken from (a) are shown at corresponding positions, two t-BLG regions are shown (empty and filled squares) to show that these t-BLG regions have similar spectra.

resonance shown in Figure 3a has now a counterpart related, in frequency, by approximately

$$\omega(^{13}C) \approx \sqrt{\frac{12}{13}}\,\omega(^{12}C)$$

Indeed, only the energy of the iTO phonon mode will change with changing the mass between the ^{12}C and the ^{13}C carbon isotopes. Their phonon dispersions (in other words, the way the phonon frequency changes with changing the phonon momentum), except by the existence of inter-layer related phonon modes, will be the same since this is determined by the electronic interactions of the system. This explains why the fwhm observed in the G′ for the $^{12}C/^{13}C$ AB-BLG system is almost twice the fwhm observed for $^{12}C/^{12}C$ AB-BLG systems.

In order to enforce our arguments, in Figure 3b, we fit the G′ band of $^{12}C/^{12}C$ AB-BLG and $^{13}C/^{13}C$ AB-BLG using four Lorentzian peaks (in a process similar to that shown in Figure 3a) corresponding to the four allowed transitions, each with an individual fwhm of 36.3 and 32.1 cm^{-1}, respectively. This is in good agreement to the values found for exfoliated $^{12}C/^{12}C$ AB-BLG samples.[26] Likewise, we fit eight peaks to the G′ peak in the $^{12}C/^{13}C$ AB-BLG. Table S1 (Supporting Information) includes all fitted peak positions. The peak positions and fwhm (32.1 cm^{-1}) of the eight fitted peaks are quite similar to the individual $^{12}C/^{12}C$ and $^{13}C/^{13}C$ fitted values. This suggests that even though the coupling between layers is relatively weak in the $^{12}C/^{13}C$ AB-BLG (such that it does not perturb the original phonon modes very significantly), this coupling is sufficient to generate a hyperbolic electronic dispersion similar to that of $^{12}C/^{12}C$ AB-BLG or $^{13}C/^{13}C$ AB-BLG samples (see Figure 3a) so that the multiple resonances can be observed.

The stacking orientation in $^{12}C/^{13}C$ AB-BLG systems was also confirmed by the observation of interlayer breathing modes, as shown in Figure 3c. In $^{12}C/^{12}C$ AB-BLG, it is already well established that the combination of modes LO + ZO′ and 2ZO appearing in the frequency range from 1650 to 1750 cm^{-1} (see the region delimited by the gray box in Figure 3c) are due to interlayer interactions.[33−37] As a matter of fact, the LO is the in-plane longitudinal mode, the ZO′ is the interlayer breathing mode (in-phase interlayer vibration) and the ZO is the out-of-plane mode. From Figure 3c, it is clear that the interlayer related features are observed only for the $^{12}C/^{13}C$ AB-BLG (red filled squares in Figure 3c) and $^{12}C/^{12}C$ AB-BLG (blue filled circles in Figure 3c). These observations are therefore a further signature of the presence of AB stacking. In addition, it is also clear that the region comprising frequencies from 1750 to 2050 cm^{-1} is similar between the AB-BLG systems in contrast to the t-BLG and SLG. The spectral shape within these frequencies for AB-BLG systems could also be envisioned as another spectroscopy signature for confirming the existence of interlayer interactions.

Large Area Identification of AB Stacked Bilayer. Furthermore, utilizing isotopically labeled bilayers, we could rapidly verify the uniformity of the stacking orientation of our bilayer graphene over large areas. The asymmetry of the G′ band is usually absent for CVD-grown $^{12}C/^{12}C$ AB-BLG while the fwhm of the G′ band alone cannot uniquely distinguish between AB and turbostratic stacking.[17] Besides TEM and SAED are very time-consuming processes that are difficult to use for large-area samples. Therefore $^{12}C/^{13}C$ BLG combined with Raman spectroscopy allow us to identify the percentage of AB-stacked regions more rapidly and accurately than other techniques. We found for our growth conditions discussed above, most of our bilayer graphene were AB-stacked; however, we also found some bilayer domains that showed a mixed orientation of AB stacking and turbostratic stacking. In Figure 4, we identify the AB-stacked regions by their fwhm of the G′ peak using a binary cutoff fwhm of 70 cm^{-1}. Other methods could also be used for differentiation; however, we chose this one for its simplicity. Figure 4 shows that many bilayer graphene domains are AB-stacked; however, we found that some bilayer graphene domains exhibited a mixed character (outlined with a red dotted line). From this 60 μm by 60 μm scan, we found that 79% of the bilayer flakes are pure AB-stacked, while the remaining bilayer flakes (21%) showed partial AB stacking (dominant) as well as pure turbostratic stacking (rare). We attributed this to perhaps variations in the monolayer growth quality. Previous reports have shown that

dx.doi.org/10.1021/nl304706j | Nano Lett. 2013, 13, 1541−1548

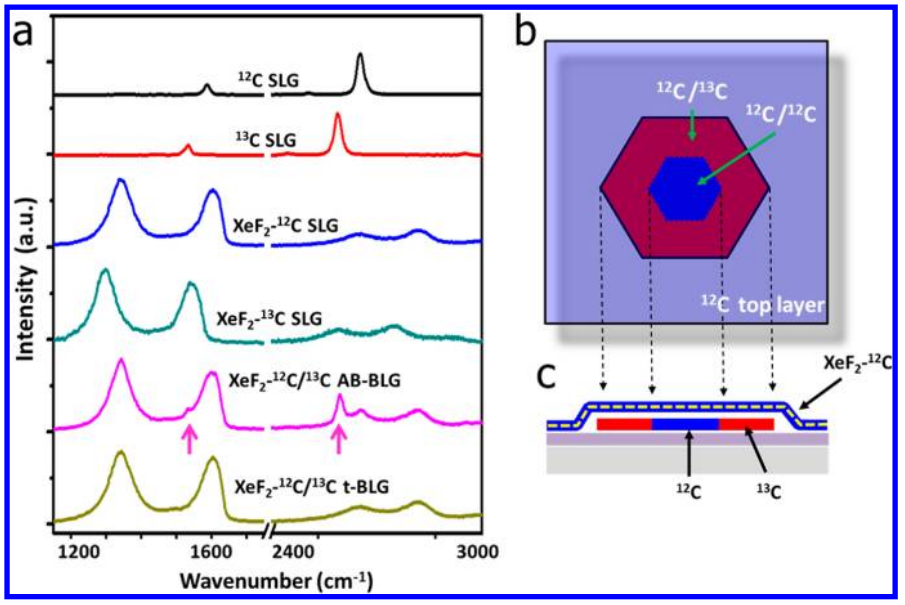

Figure 5. Raman spectroscopy of fluorinated bilayer graphene. (a) Raman spectra of pristine ^{12}C monolayer graphene (black), pristine ^{13}C monolayer graphene (red), fluorinated ^{12}C monolayer graphene (blue), fluorinated ^{13}C monolayer graphene (turquoise), fluorinated ^{12}C/^{13}C AB stacked bilayer graphene (magenta) and fluorinated ^{12}C/^{13}C turbostratic bilayer graphene (gold). (b) Schematic of the top view of ^{12}C/^{13}C bilayer graphene. (c) Schematic of the cross-section of ^{12}C/^{13}C bilayer graphene.

monolayer graphene nucleation could yield either single-crystalline or polycrystalline flakes.[38] The second layer of the bilayer flakes were assumed to be single crystalline due to their hexagonal symmetry; however, depending on the nucleation type of the first layer (single crystalline or polycrystalline) and depending on whether the second layer grows across various domains, turbostratic regions within a bilayer flake are to be expected. This suggests that the fraction of AB-stacked versus turbostratic bilayers is also strongly coupled to the growth quality of the monolayer graphene.

Fluorination. Finally, to determine the stacking sequence (whether the second layer grows on the top or below the monolayer), we used XeF_2 gas to fluorinate the exposed side of these hybrid isotopically labeled bilayer graphene samples. Since the Raman spectra for the ^{12}C and ^{13}C layers were distinct and the second layer (bilayer) is largely composed of ^{13}C, by selectively modifying the top surface we can identify whether the second layer grows on top or on the bottom. As reported by other groups, XeF_2 gas can be used to fluorinate graphene at ambient temperature, thereby creating a large amount of sp^3-bonded carbon which results in a drastic change in the Raman spectra.[39] The combination of isotopic labeling and surface sensitive modification utilizing oxygen plasma has recently been reported in identifying the stacking order of graphene grown on the inner surface of a copper envelope.[20] Here, we have developed the use of fluorination for stacking order differentiation as this method does not involve any directed plasma or focused energy that might damage both the upper and lower layers. We conducted Raman spectroscopy after fluorination and compared the spectra from the same regions as shown in Figure 5. We found dramatic changes in the Raman spectra after fluorination: increasing D peak intensity, a broadening G peak, and a decrease of the G′ peak due to doping and/or disorder. The D peaks for ^{12}C SLG and ^{13}C SLG appear at 1340 and 1294 cm^{-1} respectively. For the ^{12}C/^{13}C BLG, even though the G peak for ^{12}C graphene broadens, a small G peak for ^{13}C graphene may still be observed at 1533 cm^{-1} (indicated by an arrow) and is similar in shape to pristine ^{13}C monolayer graphene. Moreover, a sharp G′ peak is observed at 2591 cm^{-1} (indicated by an arrow) which further agrees with the presence of pristine ^{13}C graphene. These observations indicate that the ^{13}C layer deposited in the second step of the CVD process was not fluorinated while only the ^{12}C layer was fluorinated. This means the ^{13}C layer is on the bottom which was protected by the ^{12}C layer located on top. After fluorination the turbostratic sample did not show a clear G′ peak for the ^{13}C layer; however, the D peak (~1340 cm^{-1}) and G peak (~1603 cm^{-1}) both correspond to ^{12}C and the absence of similar peaks corresponding to ^{13}C still suggests that the ^{13}C layer is underneath. Hence, we conclude that the second layer originated from below, between the substrate and the first layer, as shown in Figure 5c. In ref 40, the authors investigated graphene growth on flat copper foils and suggested that the second layer grows on top of the first layer. While previous results examined the inside of the Cu enclosure,[20] we here confirm that the bilayer graphene on the outside of the copper enclosure also nucleates from underneath. This strongly suggests that the bilayer growth mechanism in the Cu enclosure case is not caused by the surrounding environment, since both the inside and outside of the enclosure have the same type of nucleation. These results also agree with previous LEEM studies on Cu foils, Ru(0001), and Ir(111).[10,41,42] The second layer growing from underneath is currently understood to be due to carbon precipitation from the bulk or diffusion of carbon underneath the top layer. Mechanisms that have been proposed for growth from above suggest that graphitic fragments could be deposited from above, serving as nucleation sites,[12] unfortunately, no stacking order is confirmed in this model. With regards to the identified stacking order of bilayers synthesized in ref 40, there is a definite difference in terms of crystalline morphology as compared to this work and ref 20. This may suggest that the mechanism of bilayer graphene growth from underneath differs from graphene growth from above.

dx.doi.org/10.1021/nl304706j | Nano Lett. 2013, 13, 1541−1548

In conclusion, we have demonstrated the growth of bilayer graphene using Cu enclosures. The bilayer graphene domain size achievable was more than 20 μm and the area coverage was ~70%. This growth method provides a facile tool to synthesize, both AB-stacked and turbostratic $^{12}C/^{13}C$ BLG. Utilizing this technique we are able to characterize not only the stacking orientation of our synthesized bilayer samples but also the stacking sequence of our bilayer using Raman spectroscopy. This information enables us to have a deeper understanding behind the growth mechanisms involved in bilayer graphene synthesis. It also serves as a rapid tool for characterizing the stacking information under various growth conditions and how they influence the stacking order. Through this new approach, we present an efficient technique to tailor both, electronic and vibrational properties of BLG and we also advance our understanding of interlayer interactions in graphene systems, which are important for technological applications of these systems that rely on phenomena such as thermal transport for infrared devices and graphene transistors. Moreover, this isotope-based technique enables a new way to study phonon interlayer interactions important for heat transfer in low dimensional systems allowing for a more efficient engineering of bilayer graphene to either dissipate heat into the substrate or out of it. This would present a major advance for nanoscale graphene-thermal electric devices.

Methods. *CVD Growth of Graphene on Cu.* The Cu foil enclosure was formed by bending a sheet of copper foil (127 μm thick, 99.9%, Alfa Aesar) and crimping the three remaining edges. For growth using isotope labeling, the following quick and effective cleaning process is employed prior to growth to increase the domain size of bilayer: Cu foil is dipped into Ni etchant (Nitric acid, Transene Company Inc.) for 30 s, immediately followed by rinsing using DI water. The growth procedure is as follows: the substrate was heated to 1000 °C under 10 sccm H_2 for 30 min for annealing. Subsequently, the CH_4 was introduced. For growth using isotope labeling, after we flowed $^{12}CH_4$ for 90 s, we stopped flowing $^{12}CH_4$ and purged the line for 5 min using 100 sccm Ar/10 sccm H_2 to reduce the chance of intermixing between the isotopes. Then we flowed $^{13}CH_4$ (99.5 atom %, Sigma-Aldrich). After growth, the furnace cover was opened and the samples were cooled under the same atmosphere as the growth condition. We grew the sample at 1035 °C and increased the growth rate to enhance the size of the bilayer domains for isotope labeling.

Transfer. We coated diluted 50:50 poly(methyl methacrylate) (PMMA, 950 A9, MicroChem, 4.5% in anisole) on the graphene on copper foil at 2500 rpm for 1 min, followed by removing copper with copper etchant (CE-100, Transene Company Inc.). Then we washed the PMMA/graphene by DI water to remove the residual copper etchant. After the PMMA/graphene film was transferred onto SiO_2/Si, the PMMA was removed by immersing the sample in acetone for more than 12 h. For PMMA/graphene samples transferred onto SiN TEM grids (Ted Pella, Inc. 2.5 μm holes), PMMA was removed by thermal annealing at 350 °C for 3 h under a 200 sccm H_2/ 200 sccm Ar atmosphere.

Characterization. The Raman spectra/mapping was taken with an acquisition time of 2 s. The laser beam spot size was 1 μm with a 100× objective and the power measured from the objective was 1 mW with a laser wavelength of 532 nm. For Figure 4, we first identified all of the bilayer regions either by optical microscopy or by ^{13}C G peak intensity (outlined in dotted lines in Figure 4). Then by analyzing the G′ peak line shape and width, we were able to differentiate between AB-stacked regions and turbostratic regions

SEM was a Zeiss Supra 40 at 5 keV acceleration voltage.

The TEM was conducted using a JEOL 2010F analytical electron microscope with acceleration voltage of 200 kV. The size for SAED was 100 nm.

Fluorination. Fluorination was carried out by a SE Tech ES-2000XM XeF_2 etcher. Exposure was done at ~2800 mTorr for 30 s at ambient temperature.

■ ASSOCIATED CONTENT

Supporting Information

Figure S1: Raman spectra of $^{12}C/^{13}C$ turbostratic bilayer, $^{12}C/^{12}C$ AB-stacked bilayer, $^{13}C/^{13}C$ AB-stacked bilayer, $^{12}C/^{12}C$ AB-stacked bilayer and $^{13}C/^{13}C$ AB-stacked bilayer (added artificially) and $^{12}C/^{13}C$ AB-stacked bilayer. Table S1: information on the fitting of bilayer graphene for Figure 3b. This material is available free of charge via the Internet at http://pubs.acs.org.

■ AUTHOR INFORMATION

Corresponding Author

*E-mail: (J.K.) jingkong@mit.edu; (P.T.A) ptaraujo@mit.edu.

Author Contributions

W.F. performed sample growth, Raman spectroscopy and TEM. A.L.H. carried out SEM. R.C. carried out the fluorination process. S.Y. assisted on the sample transfer. All authors contributed to the discussion of the data analysis and commented on the manuscript. W.F., A.L.H., and P.T.A wrote the manuscript. W.F. and A.L.H. contributed equally to this work.

Notes

The authors declare no competing financial interests.

■ ACKNOWLEDGMENTS

This work was partially supported by the National Science Foundation under award number NSF DMR 0845358 and the Graphene Approaches to Terahertz Electronics (GATE) Multidisciplinary University Research Initiative (MURI) of Massachusetts Institute of Technology (MIT)-Harvard University-Boston University through the Office of Naval Research (ONR), MSD Focus Center, and U.S. Army Research Laboratory (ARL). P.T.A. and M.S.D. acknowledge ONR-MURI-N00014-09-1-1063. M.K. acknowledges the support from GACR project P208/12/1062. M.K. acknowledges the support from GACR project P208/12/1062 and MSMT (LH13022).

■ REFERENCES

(1) Geim, A. K.; Novoselov, K. S. The rise of graphene. *Nat. Mater.* **2007**, *6* (3), 183−91.

(2) Ohta, T.; Bostwick, A.; Seyller, T.; Horn, K.; Rotenberg, E. Controlling the Electronic Structure of Bilayer Graphene. *Science* **2006**, *313* (5789), 951−954.

(3) Oostinga, J. B.; Heersche, H. B.; Liu, X.; Morpurgo, A. F.; Vandersypen, L. M. K. Gate-induced insulating state in bilayer graphene devices. *Nat. Mater.* **2007**, *7* (2), 151−157.

(4) Zhang, Y.; Tang, T.-T.; Girit, C.; Hao, Z.; Martin, M. C.; Zettl, A.; Crommie, M. F.; Shen, Y. R.; Wang, F. Direct observation of a widely tunable bandgap in bilayer graphene. *Nature* **2009**, *459* (7248), 820−823.

(5) Xia, F.; Farmer, D. B.; Lin, Y.-M.; Avouris, P. Graphene Field-Effect Transistors with High on/off Current Ratio and Large

Transport Band Gap at Room Temperature. *Nano Lett.* **2010**, *10* (2), 715−8.
(6) Tang, T.-T.; Zhang, Y.; Park, C.-H.; Geng, B.; Girit, C.; Hao, Z.; Martin, M. C.; Zettl, A.; Crommie, M. F.; Louie, S. G.; Shen, Y. R.; Wang, F. A tunable phonon−exciton Fano system in bilayer graphene. *Nat. Nanotechnol.* **2010**, *5* (1), 32−36.
(7) Bae, S.; Kim, H.; Lee, Y.; Xu, X.; Park, J.-S.; Zheng, Y.; Balakrishnan, J.; Lei, T.; Ri Kim, H.; Song, Y. I.; Kim, Y.-J.; Kim, K. S.; Özyilmaz, B.; Ahn, J.-H.; Hong, B. H.; Iijima, S. Roll-to-roll production of 30-in. graphene films for transparent electrodes. *Nat. Nanotechnol.* **2010**, *5* (8), 574−578.
(8) Wang, Y.; Tong, S. W.; Xu, X. F.; Özyilmaz, B.; Loh, K. P. Interface Engineering of Layer-by-Layer Stacked Graphene Anodes for High-Performance Organic Solar Cells. *Adv. Mater.* **2011**, *23* (13), 1514−1518.
(9) Sutter, P. W.; Flege, J.-I.; Sutter, E. A. Epitaxial graphene on ruthenium. *Nat. Mater.* **2008**, *7* (5), 406−411.
(10) Nie, S.; Walter, A. L.; Bartelt, N. C.; Starodub, E.; Bostwick, A.; Rotenberg, E.; McCarty, K. F. Growth from Below: Graphene Bilayers on Ir(111). *ACS Nano* **2011**, *5* (3), 2298−2306.
(11) Wu, Y.; Chou, H.; Ji, H.; Wu, Q.; Chen, S.; Jiang, W.; Hao, Y.; Kang, J.; Ren, Y.; Piner, R. D.; Ruoff, R. S. Growth Mechanism and Controlled Synthesis of AB-Stacked Bilayer Graphene on Cu−Ni Alloy Foils. *ACS Nano* **2012**, *6* (9), 7731−7738.
(12) Yan, K.; Peng, H.; Zhou, Y.; Li, H.; Liu, Z. Formation of Bilayer Bernal Graphene: Layer-by-Layer Epitaxy via Chemical Vapor Deposition. *Nano Lett.* **2011**, *11* (3), 1106−1110.
(13) Liu, L.; Zhou, H.; Cheng, R.; Yu, W. J.; Liu, Y.; Chen, Y.; Shaw, J.; Zhong, X.; Huang, Y.; Duan, X. High-Yield Chemical Vapor Deposition Growth of High-Quality Large-Area AB-Stacked Bilayer Graphene. *ACS Nano* **2012**, *6* (9), 8241−8249.
(14) Reina, A.; Jia, X.; Ho, J.; Nezich, D.; Son, H.; Bulovic, V.; Dresselhaus, M. S.; Kong, J. Large Area, Few-Layer Graphene Films on Arbitrary Substrates by Chemical Vapor Deposition. *Nano Lett.* **2009**, *9* (1), 30−5.
(15) Yan, Z.; Peng, Z.; Sun, Z.; Yao, J.; Zhu, Y.; Liu, Z.; Ajayan, P. M.; Tour, J. M. Growth of Bilayer Graphene on Insulating Substrates. *ACS Nano* **2011**, *5* (10), 8187−8192.
(16) Lee, S.; Lee, K.; Zhong, Z. Wafer Scale Homogeneous Bilayer Graphene Films by Chemical Vapor Deposition. *Nano Lett.* **2010**, *10* (11), 101008162231093.
(17) Kim, K.; Coh, S.; Tan, L. Z.; Regan, W.; Yuk, J. M.; Chatterjee, E.; Crommie, M. F.; Cohen, M. L.; Louie, S. G.; Zettl, A. Raman Spectroscopy Study of Rotated Double-Layer Graphene: Misorientation-Angle Dependence of Electronic Structure. *Phys. Rev. Lett.* **2012**, *108* (24), 246103.
(18) Li, X.; Cai, W.; Colombo, L.; Ruoff, R. S. Evolution of Graphene Growth on Ni and Cu by Carbon Isotope Labeling. *Nano Lett.* **2009**, *9* (12), 4268−4272.
(19) Kalbac, M.; Farhat, H.; Kong, J.; Janda, P.; Kavan, L.; Dresselhaus, M. S. Raman Spectroscopy and in Situ Raman Spectroelectrochemistry of Bilayer 12C/13C Graphene. *Nano Lett.* **2011**, *11* (5), 1957−1963.
(20) Li, Q.; Chou, H.; Zhong, J.-H.; Liu, J.-Y.; Dolocan, A.; Zhang, J.; Zhou, Y.; Ruoff, R. S.; Chen, S.; Cai, W. Growth of Adlayer Graphene on Cu Studied by Carbon Isotope Labeling. *Nano Lett.* **2013**, *13* (2), 486−490.
(21) Li, X.; Magnuson, C. W.; Venugopal, A.; Tromp, R. M.; Hannon, J. B.; Vogel, E. M.; Colombo, L.; Ruoff, R. S. Large-area graphene single crystals grown by low-pressure chemical vapor deposition of methane on copper. *J. Am. Chem. Soc.* **2011**, *133* (no. 9), 2816−9.
(22) Fang, W.; Hsu, A.; Birdwell, G.; Zakar, E.; Dubey, M.; Palacios, T.; Dresselhaus, M.; Kong, J. Growth Mechanism of Bilayer Graphene on Asymmetric Metal Catalysts. Unpublished work, 2012.
(23) Li, X.; Cai, W.; An, J.; Kim, S.; Nah, J.; Yang, D.; Piner, R.; Velamakanni, A.; Jung, I.; Tutuc, E.; Banerjee, S. K.; Colombo, L.; Ruoff, R. S. Large-area synthesis of high-quality and uniform graphene films on copper foils. *Science (New York)* **2009**, *324* (no. 5932), 1312−4.
(24) Ago, H.; Ishigami, N.; Yoshihara, N.; Imamoto, K.; Akita, S.; Ikeda, K.; Tsuji, M.; Ikuta, T.; Takahashi, K. Visualization of Horizontally-Aligned Single-Walled Carbon Nanotube Growth with 13C/12C Isotopes. *J. Phys. Chem. C* **2008**, *112* (6), 1735−1738.
(25) Horiuchi, S.; Gotou, T.; Fujiwara, M.; Sotoaka, R.; Hirata, M.; Kimoto, K.; Asaka, T.; Yokosawa, T.; Matsui, Y.; Watanabe, K.; Sekita, M. Carbon Nanofilm with a New Structure and Property. *Jpn. J. Appl. Phys.* **2003**, *42*, L1073−L1076.
(26) Meyer, J. C.; Geim, A. K.; Katsnelson, M. I.; Novoselov, K. S.; Obergfell, D.; Roth, S.; Girit, C.; Zettl, A. On the roughness of single- and bi-layer graphene membranes. *Solid State Commun.* **2007**, *143* (1−2), 101−109.
(27) Meyer, J. C.; Geim, A. K.; Katsnelson, M. I.; Novoselov, K. S.; Booth, T. J.; Roth, S. The structure of suspended graphene sheets. *Nature* **2007**, *446* (7131), 60−63.
(28) Malard, L. M.; Guimarães, M. H. D.; Mafra, D. L.; Mazzoni, M. S. C.; Jorio, A. Group-theory analysis of electrons and phonons in N-layer graphene systems. *Phys. Rev. B* **2009**, *79* (12), 125426.
(29) Yan, J.-A.; Ruan, W. Y.; Chou, M. Y. Phonon dispersions and vibrational properties of monolayer, bilayer, and trilayer graphene: Density-functional perturbation theory. *Phys. Rev. B* **2008**, *77* (12), 125401.
(30) Wang, H.; Wang, Y.; Cao, X.; Feng, M.; Lan, G. Vibrational properties of graphene and graphene layers. *J. Raman Spectrosc.* **2009**, *40* (12), 1791−1796.
(31) Malard, L. M.; Nilsson, J.; Elias, D. C.; Brant, J. C.; Plentz, F.; Alves, E. S.; Castro Neto, A. H.; Pimenta, M. A. Probing the electronic structure of bilayer graphene by Raman scattering. *Phys. Rev. B* **2007**, *76* (20), 201401.
(32) Mafra, D. L.; Malard, L. M.; Doorn, S. K.; Htoon, H.; Nilsson, J.; Castro Neto, A. H.; Pimenta, M. A. Observation of the Kohn anomaly near the K point of bilayer graphene. *Phys. Rev. B* **2009**, *80* (24), 241414.
(33) Lui, C. H.; Malard, L. M.; Kim, S.; Lantz, G.; Laverge, F. E.; Saito, R.; Heinz, T. F. Observation of out-of-plane vibrations in few-layer graphene. *Nano Lett.* **2012**, *12* (11), 5539.
(34) Sato, K.; Park, J. S.; Saito, R.; Cong, C.; Yu, T.; Lui, C. H.; Heinz, T. F.; Dresselhaus, G.; Dresselhaus, M. S. Raman spectra of out-of-plane phonons in bilayer graphene. *Phys. Rev. B* **2011**, *84* (3), 035419.
(35) Araujo, P. T.; Mafra, D. L.; Sato, K.; Saito, R.; Kong, J.; Dresselhaus, M. S. Unraveling the interlayer-related phonon self-energy renormalization in bilayer graphene. *Sci. Rep.* **2012**, *2* (1017), 1.
(36) Cong, C.; Yu, T.; Saito, R.; Dresselhaus, G. F.; Dresselhaus, M. S. Second-Order Overtone and Combination Raman Modes of Graphene Layers in the Range of 1690−2150 cm^{-1}. *ACS Nano* **2011**, *5* (3), 1600−1605.
(37) Cong, C.; Yu, T.; Sato, K.; Shang, J.; Saito, R.; Dresselhaus, G. F.; Dresselhaus, M. S. Raman Characterization of ABA- and ABC-Stacked Trilayer Graphene. *ACS Nano* **2011**, *5* (11), 8760−8768.
(38) Zhang, Y.; Zhang, L.; Kim, P.; Ge, M.; Li, Z.; Zhou, C. Vapor Trapping Growth of Single-Crystalline Graphene Flowers: Synthesis, Morphology, and Electronic Properties. *Nano Lett.* **2012**, *12* (6), 2810−2816.
(39) Robinson, J. T.; Burgess, J. S.; Junkermeier, C. E.; Badescu, S. C.; Reinecke, T. L.; Perkins, F. K.; Zalalutdniov, M. K.; Baldwin, J. W.; Culbertson, J. C.; Sheehan, P. E.; Snow, E. S. Properties of Fluorinated Graphene Films. *Nano Lett.* **2010**, *10* (8), 3001−3005.
(40) Kalbac, M.; Frank, O.; Kavan, L. The control of graphene double-layer formation in copper-catalyzed chemical vapor deposition. *Carbon* **2012**, *50* (10), 3682−3687.
(41) Nie, S.; Wu, W.; Xing, S.; Yu, Q.; Bao, J.; Pei, S.; McCarty, K. F. Growth from below: bilayer graphene on copper by chemical vapor deposition. *New J. Phys.* **2012**, *14* (9), 093028.
(42) Cui, Y.; Fu, Q.; Bao, X. Dynamic observation of layer-by-layer growth and removal of graphene on Ru(0001). *Phys. Chem. Chem. Phys.* **2010**, *12* (19), 5053−5057.